Experimental Study of High Temperature Phase Equilibria in the Iron-Rich Part of the Fe-P and Fe-C-P Systems

MICHAEL BERNHARD, PETER PRESOLY, NORA FUCHS, CHRISTIAN BERNHARD, and YOUN-BAE KANG

During the solidification of steel, phosphorus strongly segregates in the interdendritic liquid phase. In the continuous casting process, even low levels of P may have a detrimental effect on the final product quality. However, phosphorus is partly added up to 0.10 wt pct to improve the mechanical properties of advanced steel grades nowadays, *e.g.,* High-Strength Interstitial-Free (HSIF). To provide new experimental data for the development of thermodynamic databases and solidification models for P alloyed steel grades, phase equilibria in the Fe-P and Fe-C-P key systems were studied up to 1550 °C using differential scanning calorimetry (DSC) and high temperature laser scanning confocal microscopy (HT-LSCM). Special focus was placed on solid/liquid equilibrium temperatures in the Fe-rich part of the binary Fe-P system between 0.025 and 9 wt pct P. In the ternary system, three isoplethal sections with 0.10 mass pct. P, 0.20 mass pct. C and constant mass percent ratio P/C of 2 were investigated. In the latter section, HT-LSCM observations were linked with DSC signals to optically identify present phase stabilities. Particularly at [pct P] < 1, significant differences between performed measurements and calculated phase equilibrium temperatures using thermodynamic assessments from the literature were identified. In all ternary sections, the experiments indicate less influence of P on the hypo-peritectic range compared to the thermodynamic calculations.

https://doi.org/10.1007/s11661-020-05912-z

I. INTRODUCTION

PHOSPHORUS is generally known as a harmful element in steel. In the continuous casting process, the strong segregation of P during solidification may lead to internal quality problems, *e.g.* hot tear formation. Increasing amounts of carbon and other alloying elements lower the solidification temperatures and possibly change the phase transformation path in the peritectic range. As a consequence, the limited diffusivity of P along the dendritic microstructure at decreased temperatures and the low solubility of P in austenite favor the interdendritic enrichment and cause an even higher risk of crack formation in the casting process.[1–4] However, despite the detrimental effects on the product quality, phosphorus is partly added in steelmaking nowadays to improve various performance characteristics of steel: (i) P acts as the most effective solution-hardening element in the steel matrix. This strengthening mechanism is particularly used in the production of High-Strength Interstitial-Free (HSIF) steels.[5] (ii) P is added up to 0.10 mass pct. to structural steels in order to improve the atmospheric resistance.[6,7] (iii) In transformation induced plasticity (TRIP) steels, P stabilizes the retained austenite; amounts up to 0.10 wt pct are considered to show beneficial influence on the TRIP effect.[8]

Reliable phase diagram data in the high-temperature range of the ternary Fe-C-P system are essential for developing a comprehensive understanding of solidification phenomena in P alloyed steels. In the present study, high-temperature phase transformations of 37 model alloys in the Fe-P and Fe-C-P systems were investigated using differential scanning calorimetry (DSC) and high-temperature laser scanning confocal microscopy (HT-LSCM). The DSC method has already been used in previous works[9,10] to characterize the influence of alloying elements on the peritectic range and determine melting equilibrium temperatures in Fe-C-X isoplethal sections. Linking the DSC method with HT-LSCM observations is a supportive and powerful

MICHAEL BERNHARD, PETER PRESOLY, NORA FUCHS, and CHRISTIAN BERNHARD are with the Chair of Ferrous Metallurgy, Montanuniversitaet Leoben, Franz-Josef-Strasse 18, 8700 Leoben, Austria Contact e-mail: michael.bernhard@unileoben.ac.at YOUN-BAE KANG is with the Graduate Institute of Ferrous Technology, Pohang University of Science and Technology, Kyungbuk 37673, Pohang, Republic of Korea.

Manuscript submitted February 27, 2020.
Article published online July 23, 2020

tool to gain additional information on present phase stabilities in the peritectic region and confirm the interpretation of the DSC signal.[9]

The first part of this work deals with the reinvestigation of phase equilibria in the binary Fe-P subsystem in the range 0.025 to 9 mass percent P. Due to the lack of experimental literature data at low P compositions, special focus was placed on compositions < 1 mass percent P. In the second part, three isoplethal sections in the Fe-C-P system were investigated. Model alloys with Fe-C-0.10 wt pct P and Fe-0.20 wt pct C-P were produced according to the initial phosphorus composition of P alloyed steel grades, whereas the additional section with constant P/C mass percent ratio of 2 corresponds to typical enrichments of C and P during solidification. In the latter section, selected DSC measurements were linked with HT-LSCM observations to visually identify phase stabilities and estimate transformation temperatures. The purpose of the present work is to provide new experimental data for the further improvement of thermodynamic databases and solidification models for P alloyed steels.

II. LITERATURE REVIEW

A. *Binary Fe-P System*

As generally accepted from Okamoto,[11] the binary Fe-P system consists of three solution phases - liquid, fcc (γ) and bcc (α, δ)—and three stoichiometric compounds (Fe_3P, Fe_2P and FeP). Although the existence of higher order phosphides (FeP_2 and FeP_4) was reported in previous works[12–15] the phase diagram on the P-rich side is still unknown.[11] A large amount of experimental phase diagram data was summarized in Okamoto's work.[11] However, depending on the reported experimental technique and the trace element level in the investigated alloys, the published measurements significantly differ. Particularly, for bcc/liquid equilibria in the Fe-rich part, high deviations were identified in the available data sets.[16–22] Solid phase equilibria in the fcc/bcc gamma loop region were studied in References 23 through 25; the maximum solubility of P in fcc was found to be 0.31 wt pct[24] or 0.265 wt pct[25] at 1150 °C. Alloys with phosphorus content higher than 0.69 wt pct[24] or 0.59 wt pct,[25] respectively, do not show a bcc/fcc phase transformation in solid state. The solubility of P in bcc between 550 °C and 1200 °C was reported in References 26 through 29; a maximum value of 2.8 mass pct. at the temperature 1048°C is generally accepted.[11] The eutectic composition in the Fe-P system is 10.2 mass pct. P.[11] From literature, various thermodynamic assessments of the binary Fe-P system are available.[30–36] However, for the present work only assessments of the Fe-P systems that are being used in a consistent description of the ternary Fe-C-P system are of particular interest. Hence, the work of Shim *et al.*[32] was considered for the discussion of the present experimental data. The calculated binary Fe-P phase diagram along with experimental data from the References 16 through 29 is shown in Figure 1.

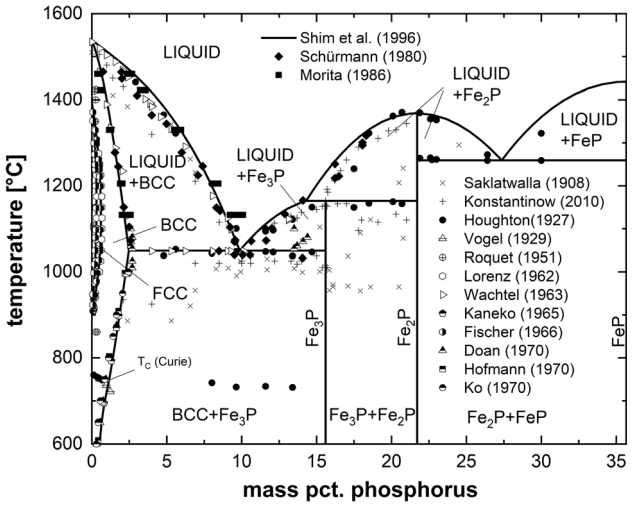

Fig. 1—Calculated binary Fe-P phase diagram according to Shim *et al.*[32] up to composition of FeP along with experimental data from References 16 through 29.

B. *Ternary Fe-C-P System*

An extensive literature review of phase equilibria, thermodynamic properties and crystallographic data in the Fe-C-P system was presented by Perrot.[37] However, since literature data on low amounts of phosphorus is limited, only melting equilibria of Schürmann *et al.*[38] was taken to critically evaluate the present results in the [pct P]/[pct C] = 2 section. From literature, two consistent thermodynamic descriptions of the ternary Fe-C-P system are available.[31,39] In both studies, the authors considered their own optimization of the Fe-P binary subsystems[31,32] and the most widely used Fe-C thermodynamic description of Gustafson.[40] Shim *et al.*[39] already reported higher correlation with experimental data than that found in Gustafson's study.[31] Therefore, the assessments of Shim *et al.*[32,39] were adopted to discuss the present results in the Fe-P binary and Fe-C-P ternary system. All stable phases in the ternary Fe-C-P system and their crystallographic data are summarized in Table I.

III. EXPERIMENTAL TECHNIQUES

A. *Sample Preparation and Chemical Analysis*

All samples investigated by DSC and HT-LSCM were produced in a high-frequency remelting (HFR) furnace "Lifumat-Met-3.3-Vac" from Linn High Therm GmbH. Pure technical iron cylinders (99.9 mass pct. Fe), high purity red phosphorus powder (98.9 pct, Alfa Aesar, LOT# U01C005), high purity aluminum wire (for deoxidation) and a previously prepared Fe-4.4 pct C alloy were used as the starting materials. The eutectic Fe-4.4 pct C alloy was melted in a 20 kg induction furnace using synthetic desulfurized graphite powder (Alfa Aesar, LOT# BCBB5882). In order to guarantee controlled melting in the HFR process, a hole was drilled in the 50 g iron cylinders and filled with the amount of alloying elements according to the defined

Table I. Crystallographic Data of Stable Phases Found in the Fe-C-P System[11,37]

Phase	Pearson Symbol	Space Group	Strukturbericht	Prototype	Denoted in Text
Liquid	—	—	—	—	liquid
(γFe)	cF4	$Fm\bar{3}m$	A1	Cu	fcc
(αFe), (δFe)	cI2	$Im\bar{3}m$	A2	W	bcc
Fe_3P	tI32	$I\bar{4}$	$D0_e$	Ni_3P	—
Fe_2P	hP9	$P\bar{6}2m$	C22	Fe_2P	—
FeP	oP8	$Pna2_1$	—	MnP	—
FeP_2	oP6	Pnnm	C18	FeS_2 (marcasite)	—
FeP_4	mP30	$P2_1/c$	—	FeP_4	—
(P) white	c**	—	—	(P) white	P
Fe_3C	oP16	Pnma	$D0_{11}$	Fe_3C	Fe_3C
C (gr.)	hP4	$P6_3/mmc$	A9	C (gr.)	C

chemical composition. As powder-based red phosphorus may show high surface affinity to oxygen, samples with a higher P amount ([pct P] > 0.1) were deoxidized with 0.03 mass pct. Al. The melting process was carried out in alumina crucibles under argon 5.0 over-pressure atmosphere. After two minutes of homogenization by inductive bath movement, the melt was centrifugally casted into a copper mold. The final chemical analysis of each sample was determined by (i) optical emission spectroscopy (OES) for alloys with [pct P] ≤ 0.1. The OES of type OBLF QSG 750 was calibrated with internal standards up to 0.35 pct P. (ii) In case of [pct P] > 0.1, the samples were analyzed with an X-ray fluorescence (XRF) spectrometer Thermo Fisher XRF ARL 9900. The XRF spectrometer was calibrated up to 4 mass pct. P with results of inductively coupled plasma (ICP) - OES. (iii) For alloys with P ≥ 6 mass pct. the chemical analysis was determined by ICP-OES. For detailed chemical analysis and trace element levels of all investigated samples, the authors refer to the electronic supplementary material (ESM).

B. *Differential Scanning Calorimetry (DSC)*

Differential scanning calorimetry is a proven method to record phase transitions associated with an exothermic or endothermic enthalpy change. Detailed information on the DSC technique and its application to the characterization of high temperature phase transformations in Fe-C-X (X = Si, Mn, Al, …) systems can be found in the References 9, 10, 41, 42. Measurements for the present study were performed in a NETZSCH DSC 404F1 Pegasus with an Rh furnace (T_{max} = 1.650 °C) and a platinum DSC sensor with type S thermocouples. Al_2O_3 crucibles (85 μl) and lids were used for all experiments; in each measurement the reference was an empty crucible. The protective tube of the Rh furnace was purged permanently with Ar 5.0 (purity 99.999 pct). In order to minimize oxygen levels at temperatures higher than 350 °C, a thermally active zirconium getter was placed directly below the DSC sensor. The experimental setup was calibrated by measuring the melting points of NETZSCH's standards of pure metals In, Bi, Al, Ag, Au, Ni and Co.

The DSC signal depends strongly on (i) the sample mass, (ii) the amount of heat change during the phase transformation and (iii) the heating rate (HR) applied in the scanning mode.[42] For all experiments, a relatively low sample mass of 50 mg was selected to guarantee near-equilibrium conditions without any temperature gradients inside the sample. Moreover, measurements with small samples result in a sharp peak separation in the DSC signal. Particularly during strong exothermic or endothermic phase transformations, *e.g.* solid-liquid equilibria, the transformation peaks have to be corrected from the scanning mode signal to obtain the equilibrium value. Within the classical method,[43] the peak temperatures are determined at various heating rates using new samples for each measurement. Finally, the HR-dependent peak temperature is extrapolated to an HR of zero °C/min, which corresponds to the equilibrium value. However, this method is very time consuming and a large number of samples have to be prepared. NETZSCH's Tau-R software[44,45] provides a very effective way to exclude the setup influence on the DSC signal in order to calculate the equilibrium data from a single measurement. In the present study, the validity of the Tau-R method was critically evaluated by taking the example of a hypo-peritectic Fe-0.136 pct C-0.105 pct P alloy. For detailed information on the interpretation of DSC signals to determine phase transformation temperatures in alloys (*e.g.* definition of "onset" and "peak" temperatures) the authors like to refer to the NIST Recommended Practice Guide.[42] The "onset" temperature represents the first deviation from the stable base line and is associated with the beginning of a phase transformation. A "peak" temperature is defined as a local maximum of the DSC signal and generally represents the end of the respective phase transformation. In a first step, the classic HR variation with 5, 7.5, 10, 15 and 20 °C/min was applied to determine the equilibrium temperatures. The results of the HR variation are presented in Figure 2. From Figure 2(a) it can be seen that increasing heating rates result in a stronger intensity of the DSC signal but shift the liquidus temperature (T_L) and the end of the peritectic reaction ($T_{P,E}$) to higher temperatures. The numerical values of all phase transformation

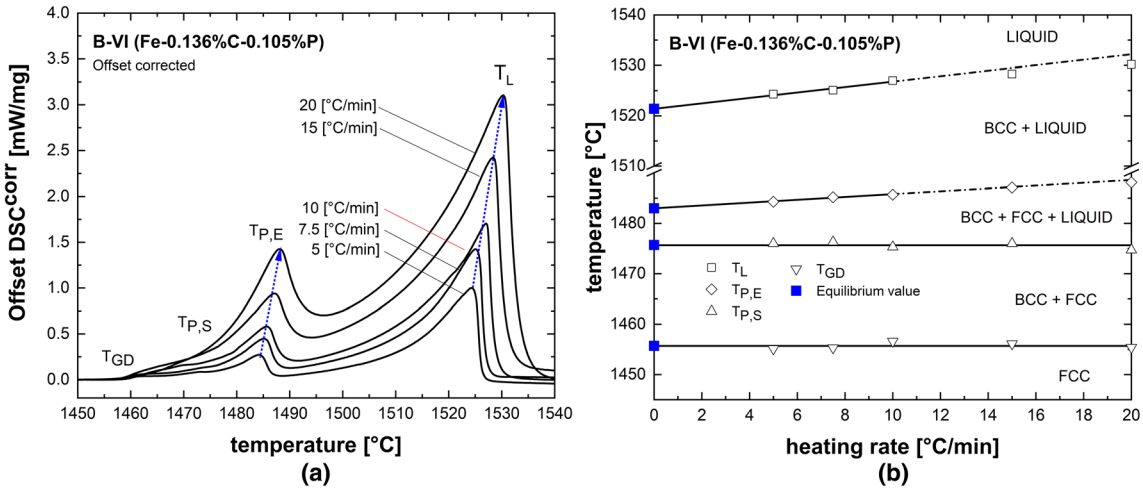

Fig. 2—DSC signal of the alloy B-VI (Fe-0.136 pct C-0.105 pct P) corrected to the baseline 0.0 mW/mg using different heating rates of 5, 7.5, 10, 15 and 20 °C (*a*) and analysis of the numerical results depending on the heating rate to determine the equilibrium temperatures at 0 °C/min (*b*).

temperatures are plotted against the HR in Figure 2(b). As expected, no influence of the HR was observed for "onset" temperatures (fcc/bcc transformation start temperature T_{GD} and peritectic start temperature $T_{P,S}$). Hence, the final values of T_{GD} = 1455.7 °C and $T_{P,S}$ = 1475.7 °C are given as average temperatures. In case of $T_{P,E}$ and T_L, a clear dependence on the heating rate is evident from Figure 2(b). In the present DSC set-up, a linear correlation exists only from 0 to 10 °C/min, whereas at higher HR of 15 and 20 °C/min, the DSC system responds with a delay and the results of T_L and $T_{P,E}$ show a parabolic function. In terms of accuracy and reliability of the results, the HR variation for the DSC set-up used is only valid in the range of 0 to 10 °C/min and the linear extrapolation to 0 °C/min gives T_L = 1521.4 °C and $T_{P,E}$ = 1483 °C.

Since the Tau-R calibration is only valid for a defined heating rate, a suitable HR has to be selected for the entire experimental study. Based on the results of the HR variation, the authors applied 10 °C/min within all measurements: (i) between 0 and 10 °C/min the peak temperatures show a linear correlation with the HR, (ii) a short residence time in the high temperature range (> 1450 °C) reduces aging of the Pt/Rh thermocouples of the DSC sensor, (iii) the measurement time is minimized by guaranteeing a sufficient intensity of the DSC signal at the same time and (iv) a heating rate of 10 °C/min accords with suggestions from Reference 43. For the Tau-R calibration, a comprehensive evaluation of the calibration measurements (In to Co) was performed to determine the temperature-dependent time constant (Tau) and the thermal resistances (R) of the DSC set-up. The performed Tau-R calculation of the 10 °C/min measurement and the actual DSC signal are plotted for comparisons in Figure 3. It can be seen that the equilibrium peak temperatures of the Tau-R method show a significant difference from the results in the scanning mode (ΔT_L = 6 °C and $\Delta T_{P,E}$ = 3°C), whereas the onset temperatures T_{GD} and $T_{P,S}$ are not affected by the Tau–R correction. Finally, the numerical results of

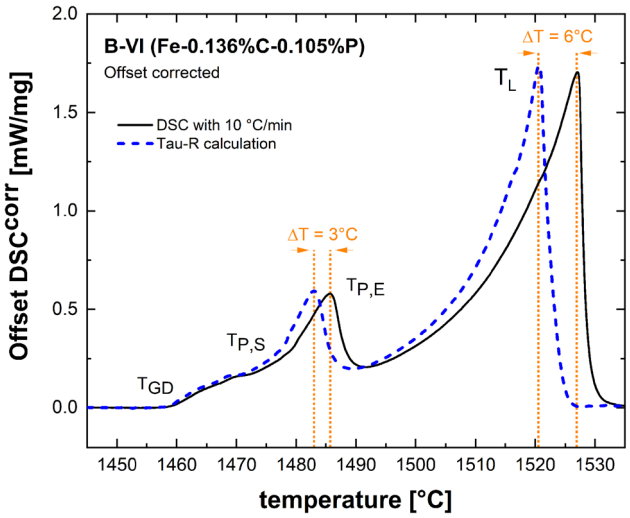

Fig. 3—Comparison of the scanning mode signal and the Tau-R calculation of alloy B-VI (Fe-0.136 pct C-0.105 pct P) for the 10°C/min measurement.

the HR variation and the Tau–R method are summarized in Table II. The equilibrium values T_{GD} = 1455.7 °C and $T_{P,S}$ = 1475.7 °C from the heating rate variation are in excellent agreement with the Tau–R calculation (T_{GD} = 1455.6 °C and $T_{P,S}$ = 1474.1 °C). The peak temperature $T_{P,E}$ = 1483 °C is exactly reproduced and the deviation of T_L is within ± 1 °C, which is below the typical errors of ± 1.5 °C in DSC measurements.[9] The really good correlation between both methods confirms the application of the Tau–R software in the present study.

The detailed time-temperature-gas programs for the DSC analysis are visualized in Figure 4. For each alloy, a "slow" temperature cycle was defined for the first measurements and a "rapid" program for the second ones. Both DSC programs start with three evacuations and purging cycles followed by 45 minutes of intensive purging with 150 ml/min Ar at 25 °C. In order to

Table II. Numerical Results of the Heating Rate Variation and the Tau-R Calculation for Alloy B-VI(Fe-0.136 Pct C-0.105 Pct P)

Temperature	Phase Equilibrium	Heating Rate Variation in the DSC					Equilibrium Temperatures		
		5 [°C/min]	7.5 [°C/min]	10 [°C/min]	15 [°C/min]	20 [°C/min]	Regression 0 [°C/min]	R^2	Tau-R [°C]
Onset: T_{GD}	(fcc → fcc + bcc)	1455.1	1455.3	1456.6	1456.1	1455.4	1455.7[a]	—	1455.6
Onset: $T_{P,S}$	(fcc + bcc → fcc + liquid + bcc)	1476.0	1476.3	1475.3	1476.0	1474.7	1475.7[a]	—	1474.1
Peak: $T_{P,E}$	(fcc + liquid + bcc → liquid + bcc)	1484.3	1485.2	1485.7	1487.1	1488.1	1483.0[b]	0.97	1483.0
Peak: T_L	(bcc + liquid → liquid)	1524.3	1525.1	1527.0	1528.3	1530.2	1521.4[b]	0.95	1520.7

[a]Onset temperature shows only a minor dependency on the heating rate; the equilibrium value is averaged from 5 to 20 °C/min measurements.
[b]Peak temperature is dependent on heating rate; the equilibrium value is linearly extrapolated to a heating rate of 0 °C/min.

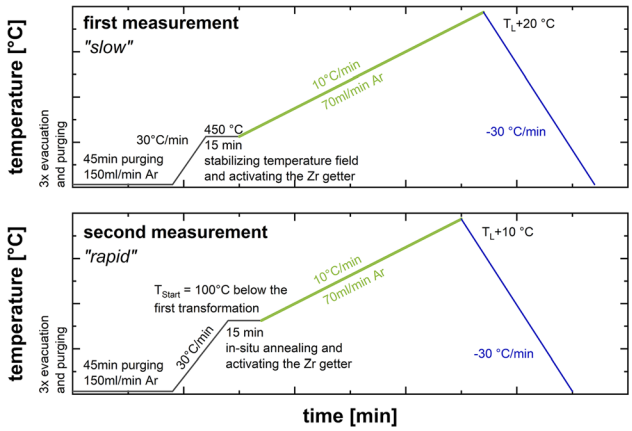

Fig. 4—Time–Temperature–Gas program of the DSC measurements.

activate the Zr getter, the first heating is carried out quickly (30 °C/min) to reach temperatures above 350 °C. The "slow" measurement starts at 450 °C with an isothermal segment for 15 minutes to activate the Zr getter and stabilize the temperature field in the DSC. Then, the actual measurement starts with a constant heating rate of 10 °C/min and an argon flow rate of 70 ml/min up to 20°C above the expected liquidus temperature. Based on the analysis of the "slow" temperature cycle, the "rapid" program starts at 100 °C below the first detected phase transformation using a new sample. The typical start temperature is between 600 and 700 °C. In comparison with the "slow" measurement, the starting segment is carried out at a significantly higher temperature. During the 15 min isothermal segment, the Zr getter is activated and the sample is annealed in-situ in order to favor diffusion equalization of alloying elements in the sample matrix. Again, the actual measurement is performed with an HR of 10 °C/min and 10 °C superheating above T_L. During cooling from T_L to room temperature (− 30 °C/min) under pure atmosphere, strong nucleation phenomena may result in remarkable supercooling of the phase transformation, particularly in the case of small sample masses.[43,46] Since the results were not reproducible, the cooling cycle was not considered in the evaluation of the DSC signal. To compensate aging of the Pt/Rh thermocouples of the DSC sensor, recalibration of the DSC was carried out after every ten measurements with Ag and Co.

It has to be noted that the experimental methodology presented focuses particularly on a highly accurate determination of the phase transformation temperatures, but not on measurements of the Cp (T) values. Hence, increased deviations of more than 10 pct have to be considered in the change of heat. Standard deviations of the evaluated phase transformation temperature from at least two independent measurements can be found in the ESM. In general, the authors suggest typical errors of ± 5 °C for solid-solid transitions with only minor change in heat and ± 2 °C for solid-liquid phase transformations. The error bars are similar to the previous investigations in Reference 9.

C. *In Situ Observations of Phase Transformations Using HT-LSCM*

To successfully determine the peritectic range of isoplethal Fe-C-X sections by means of the DSC method, a number of samples with varying carbon content are required to reconstruct the high temperature phase diagram. However, within measurements of individual alloys and particularly at carbon compositions between 0.12 and 0.18 mass pct., difficulties may arise in assigning the peritectic peak detected in the DSC signal to a hypo-peritectic phase transformation path, where fcc + bcc ↔ fcc + bcc + liquid, or a hyper-peritectic behavior, where fcc + liquid ↔ fcc + bcc + liquid. In such cases, high temperature laser scanning confocal microscopy (HT-LSCM) can be a valuable tool to define the phase stabilities within the observed temperature range.[9] HT-LSCM enables real time monitoring of microstructure changes by combining laser scanning confocal optics and an infrared heating furnace. Due to the special set-up, high resolution images can be recorded up to the liquid state. A detailed description of the HT-LSCM method can be found in the References 47 through 50.

Within the present work, two alloys selected from an isoplethal section were examined in an HT-LSCM type VL2000DX-SVF17SP from Lasertec to (i) investigate phase stabilities in the peritectic phase equilibrium and (ii) characterize the solidus temperature of a

hyper-peritectic alloy. Therefore, small samples of 5 × 5 × 1.5 mm were cut, ground and polished using the same basic material used for the DSC analysis. For the experiments, the samples were placed on the sample holder in the gold coated, elliptical HT furnace followed by an evacuation of the furnace chamber and flushing with high purity Ar. All samples were heated rapidly (+100°C/min) from RT to a holding temperature of at least 50 °C below the specific phase transformation start temperature determined by the DSC measurements. After annealing for 2 minutes, further heating was performed using a low-heating rate of 10 °C/min to a defined end temperature. Final cooling to RT was done using a cooling rate of − 400 °C/min. Temperature control is performed using a type S thermocouple situated at the bottom of the sample holder. In order to determine the exact temperature value of the sample surface, temperature referencing must be executed before every experimental campaign using an external thermocouple welded to the test-sample surface. Throughout the experiment, a video is recorded with a maximum frame rate of 60/s, enabling detailed studies of occurring microstructure changes post experimentally.

IV. RESULTS AND DISCUSSION

All thermodynamic calculations were performed with the thermochemical software FactSage.[51] In order to provide a better overview of the present results, tables in this chapter summarize the average phase equilibrium temperatures higher than 900 °C and the determined Curie Temperature (T_C) along with the chemical compositions of the main elements C and P. For detailed information on trace element levels in the samples, determined phase transformation temperatures below 900 °C and standard deviations of measured phase transformation temperatures, the authors refer to the supplementary Table S-I, Table S-II, Table S-III and Table S-IV.

A. *Phase Equilibria in the Binary Fe-P System*

The results of the DSC analysis for all binary Fe-P alloys are given in Table III. Phase equilibrium temperatures denoted with "-[a]" were not accurately measureable due to the limited resolution of the DSC method in the solid fcc/bcc equilibrium region. Phase transformations marked by "-[b]" are not present in the assessment of Shim *et al.*[32] and were not detected in the DSC signal.

The calculated iron-rich part of the Fe-P system[32] up to 14 mass pct. P along with the DSC results and experimental data from References 16 through 29 is given in Figure 5. Within the literature research, a lack of experimental melting equilibrium data was identified at [pct P] < 1. In this composition range, the precise knowledge of the solidus temperature T_S and liquidus temperature T_L is of particular importance to characterize the influence of P on solidification phenomena in steel, *e.g.,* microsegregation. In the present study, DSC analysis of samples with 0.026 to 1.18 mass pct. P (A–I to A–XI, see Table III) shows significant lower melting equilibrium temperatures than those predicted by Shim *et al.*[32] At 1 mass pct. P, the maximum deviations are $\Delta T_{S,max}$ = 50 °C and $\Delta T_{L,max}$ = 10 °C at the liquidus phase boundary. With an increasing amount of P (1 to 2.5 mass pct.), the measured solidus temperatures become more consistent with the calculated ones.[32]

Table III. Chemical Composition and Determined Phase Equilibrium Transformation Temperatures of Investigated Fe-P Binary Alloys

Alloy	P [Mass Pct]	Curie T_C [°C]	$\alpha+\gamma\rightarrow\gamma$ [°C]	$\gamma\rightarrow\alpha+\gamma$ [°C]	$\alpha+\gamma\rightarrow\alpha$ [°C]	$\alpha\rightarrow\alpha$ + Liquid [°C]	$\alpha+Fe_3P\rightarrow\alpha$ + Liquid [°C]	Liquidus [°C]
A-I	0.026	765.9	924.4	1389.4	1400.3	1527.5	—[b]	1535.1
A-II	0.044	765.2	937.0	1377.7	1385.9	1523.8	—[b]	1534.9
A-III	0.102	763.8	958.2	1367.7	1380.8	1513.3	—[b]	1532.4
A-IV	0.147	767.0	999.4	1341.9	1359.0	1504.7	—[b]	1529.1
A-V	0.322	757.2	—[b]	—[b]	1320.2	1474.6	—[b]	1525.3
A-VI	0.419	758.5	—[b]	—[b]	1272.4	1454.0	—[b]	1520.5
A-VII	0.480	756.9	—[b]	—[b]	—[a]	1450.7	—[b]	1520.9
A-VIII	0.660	751.8	—[b]	—[b]	—[a]	1420.2	—[b]	1515.0
A-IX	0.700	751.6	—[b]	—[b]	—[b]	1407.6	—[b]	1512.8
A-X	0.970	742.7	—[b]	—[b]	—[b]	1348.9	—[b]	1502.6
A-XI	1.180	738.5	—[b]	—[b]	—[b]	1321.5	—[b]	1497.1
A-XII	1.980	720.1	—[b]	—[b]	—[b]	1189.5	—[b]	1468.1
A-XIII	2.300	721.5	—[b]	—[b]	—[b]	1108.3	—[b]	1452.4
A-XIV	3.700	745.9	—[b]	—[b]	—[b]	—[b]	1039.7	1405.1
A-XV	5.870	748.6	—[b]	—[b]	—[b]	—[b]	1042.1	1316.2
A-XVI	6.480	748.5	—[b]	—[b]	—[b]	—[b]	1039.1	1273.9
A-XVII	7.570	748.5	—[b]	—[b]	—[b]	—[b]	1038.8	1206.2
A-XVIII	9.080	748.6	—[b]	—[b]	—[b]	—[b]	1037.2	1134.8

[a]Not accurately measurable with the DSC method.
[b]Not present according to DSC and thermodynamic assessment of the Fe-P system[32]

As evident in Figure 5, the experiments indicate that P has a stronger effect on decreasing the liquidus temperature of bcc along the whole composition range. The reconstruction of the phase boundary lines in the bcc + liquid + Fe_3P equilibrium using the present DSC data gives maximum solubility of P in bcc of 2.7 mass percent at the eutectic temperature of 1041 °C, whereas the eutectic composition is 10.26 mass pct. P. These results are in very good agreement with the generally accepted values from Okamoto.[11] In comparison with experimental melting data from References 16 through 22, the DSC measurements show high correlation with the most recently published equilibration data of Morita and Tanaka.[22] However, in their work, the determined amounts of P in bcc and liquid using microprobe analysis are strongly deviating. Hence, the present results are more reliable in order to accurately model the solidus and liquidus phase boundaries in future thermodynamic modeling work regarding the Fe-P system.

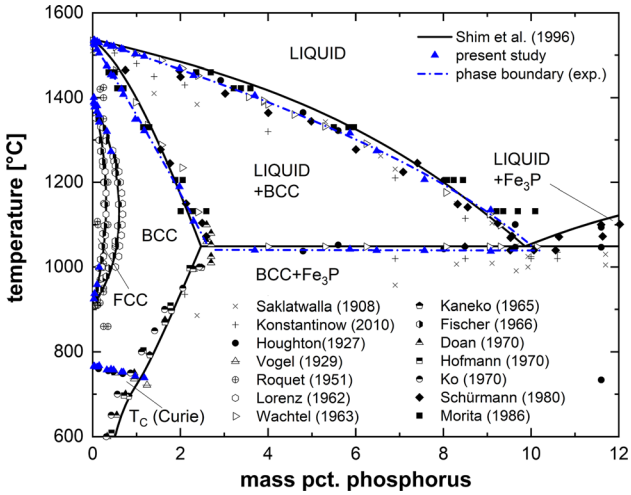

Fig. 5—Calculated iron-rich part of the Fe-P system according to the thermodynamic assessment of Shim *et al.*[32] along with the present results. Experimental literature data are taken from Refs. 16–29.

The gamma loop region of the Fe-P system is shown in Figure 6(a). In general, two trends of P solubility in fcc and bcc exist according to the literature data.[23–25] The study of Roquet and Jegadan[23] is in agreement with the work of Lorenz *et al.*[24], whereas the present results correlate with the measurements of Fischer *et al.*[25]. Although Lorenz *et al.*[24] and Fischer *et al.*[25] used the same experimental equipment, the maximum solubility of P in fcc and bcc differ from each other. The deviation can be assigned to the trace element levels of fcc stabilizing elements (C, Mn, N) in the samples produced. Even small amounts of carbon increase the P solubility in fcc and will shift the gamma loop to higher amounts of P. As given in the supplementary Table S-I and Table S-III, alloys investigated in the present study show very low amounts of impurity elements. Similar chemical analysis was reported in the work of Fischer *et al.*[25] (C ≤ 50 ppm, Si ≤ 50 ppm, Mn ≤ 10 ppm, S ≤ 50 ppm, N ≤ 40 ppm). Hence, these data sets[25] are considered as the most reliable for calculating solid state equilibrium between fcc and bcc. The assessment of Shim *et al.*[32] is in reasonable agreement with the present study, but inconsistencies in selected data from References 24, 25 were pointed out, which should be resolved in future thermodynamic assessments. The measured critical temperature T_C (Curie temperature) of the bcc solution phase as a function of the P content along with experimental data from References 18, 19 is plotted in Figure 6(b). In all studies, a decrease in the Curie temperature at higher P content was observed. Although the work of Shim *et al.*[32] reproduces the present results satisfyingly well up to 0.50 mass pct. P, remarkable differences (ΔT_C = 10 °C)

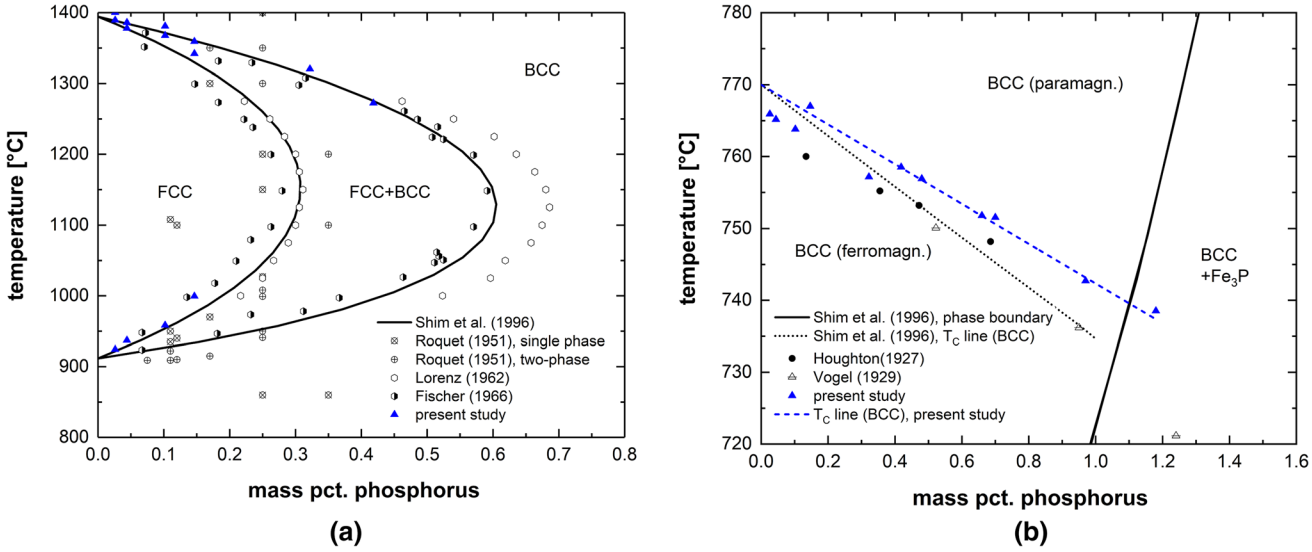

Fig. 6—Gamma loop in the Fe-P system (*a*) and T_C line in bcc (*b*) according to the thermodynamic assessment of Shim *et al.*[32] along with the present results. Experimental literature data are taken from Refs. 18, 19, 23 through 25.

can be found at compositions close to the bcc/bcc + Fe_3P phase boundary.

B. *Isoplethal Sections Fe-C-0.10 pct P and Fe-0.20 Pct C-P*

In general, the peritectic range of the binary Fe-C system can be divided into four different phase transformation paths according to the characteristic points c_A, c_B and c_C.[9,10] At C content lower than c_A = 0.09 mass pct. C,[40] steel solidifies/melts in bcc-Fe structure. Between c_A and c_B = 0.17 mass pct. C[40] the peritectic transformation coincidences with the final solidification/first melting of the alloy. From c_B to 0.53 mass pct. C (= c_C,[40]) the peritectic transformation takes place in the solid/liquid two-phase region. In case of [pct C] > 0.53 mass pct., the steel melts/solidifies in fcc-Fe structure. The phase transformation paths I - IV are summarized in Table IV. In isoplethal Fe-C-X (X = Si, Mn, Al, …) systems, the alloying element X may significantly shift the characteristic points depending on acting as bcc stabilizing element (*e.g.* Si, Al) or as fcc stabilizing element (*e.g.* Mn).[9,10]

Numerical results of the DSC measurements in the isoplethal sections Fe-C-0.10 pct P and Fe-0.20 pct C-P are summarized in Table V and represented graphically in Figures 7(a) to (c). Depending on the carbon content, the experimentally determined phase transformations in the peritectic range of the Fe-C-P systems can be divided into four different paths, as follows[9,10]:

- Samples B-I to B-III (0.004 to 0.059 mass pct. C) show separated solid fcc→bcc transformation and melting of the bcc phase (“Path I”) in the DSC signal. The amount of carbon is to the left of the characteristic point c_A.
- Samples B-IV to B-VI (0.096 - 0.136 mass pct. C) and B-VII to B-IX (0.203 to 0.378 mass pct. C) show a peritectic peak during melting. Between 0.096 and 0.136 mass pct. C, the measured fcc→fcc + bcc phase transformation start temperature continuously increases with increasing carbon content, whereas the peritectic start temperature (fcc + bcc→fcc + liquid + bcc) decreases. Therefore, samples B-IV to B-VI are identified as “hypo-peritectic” alloys (“Path II”) between points c_A and c_B.
- In the composition range 0.230 to 0.378 mass pct. C, the investigated samples B-VII to B-IX show a decrease in the solidus temperature (fcc→fcc + liquid) and a slight increase in the peritectic start temperature (fcc + liquid→fcc + liquid + bcc). B-VII to B-IX are “hyper-peritectic” and correspond to “Path III” between the characteristic points c_B and c_C.
- Samples B-X to B-XII (0.69 to 1.38 mass pct. C) only show a melting peak of the fcc phase, defined as “Path IV.” The carbon content is to the right of c_C.
- Based on the observations in the Fe-C-0.10 pct P section, the phase transformations of the samples investigated in the Fe-0.20 pct C-P system (C-I to C-III) can be assigned to “Path III.”

Table IV. Phase Stabilities in the Peritectic Range of the Fe-C System[9,10]

Path	Position	Phase Stabilities	Characteristics
I	left of “c_A”	$L \leftrightarrow L + bcc \leftrightarrow bcc \leftrightarrow bcc + fcc \leftrightarrow fcc$	primary bcc-Fe solidification/melting
II	between c_A and c_B (hypo-peritectic)	$L \leftrightarrow L + bcc \leftrightarrow bcc + fcc \leftrightarrow fcc$	peritectic transformation coincides with the final solidification/first melting
III	between c_B and c_C (hyper-peritectic)	$L \leftrightarrow L + bcc \leftrightarrow L + fcc \leftrightarrow fcc$	peritectic transformation occurs in the solid/liquid two-phase region
IV	right of c_C	$L \leftrightarrow L + fcc \leftrightarrow fcc$	primary fcc-Fe solidification/melting

The pre-identification of hypo-peritectic steel compositions (liquid + bcc→bcc + fcc) is essential for guaranteeing a successful process control in continuous casting. Steel grades in the hypo-peritectic range show strong contraction behavior during solidification that causes non-uniform shell formation, mold-level fluctuations, a higher risk of crack formation and in the worst case, break outs.[52–54] The experimentally determined hypo-peritectic carbon composition at 0.10 mass pct. phosphorus is between 0.084 and 0.147 mass pct. carbon. Shim *et al.*[39] underestimated the stability of the liquid phase, which results in a hypo-peritectic range of carbon content between 0.08 to 0.185 mass pct. C. Furthermore, it is evident from Figures 7(a) through (c) that the thermodynamic assessment proposed by Shim *et al.*[39] results in a higher solidus temperature, as found in the present experiments. At the liquid/fcc equilibrium, the difference of T_S is even more pronounced (25 °C) than at the bcc/liquid equilibrium (10 °C). As the same deviations were also identified in the binary Fe-P system, the systematic difference in the solidus temperature may be attributed to the thermodynamic description of the liquid phase in the binary system.

C. *Linking the DSC Method and HT-LSCM in the Isoplethal Section with Mass Percent Ratio P/C of 2*

The phase equilibrium temperatures measured in the isoplethal Fe-C-P section with a ratio of [pct P]/[pct C] equals 2 are summarized in Table VI. Temperatures denoted with "(a)" were determined by the DSC method and values marked with "(b)" by HT-LSCM analysis. Since the [pct P]/[pct C] ratio in the investigated samples varies between 1.88 and 2.5, all phase diagrams[39] in this chapter were performed for two different [pct P]/[pct C] ratios of 2 and 2.5.

Figures 8(a) and (b) show the DSC signals of samples D-I and D-II, the present results along with thermodynamic calculations[39] and the HT-LSCM observations. The DSC offset was corrected to the baseline of 0.0 mW/mg and the DSC signal is presented considering the Tau-R calculation as described in Chapter 3.2.

During the heating of alloy D-I (0.17 pct C-0.43 pct P), first clear deviations from the DSC baseline can be found at 1359.1 °C. At 1416.9 °C the peritectic reaction starts, which is completed at 1456.6 °C. The DSC signal peak at 1507 °C corresponds to the liquidus temperature of the bcc phase. As can be seen in the phase diagram of Figure 8(a), the carbon amount of 0.17 pct C in alloy D-I is very close to the change of the transformation sequence from fcc→fcc + bcc ("hypo-peritectic") to fcc→fcc + liquid ("hyper-peritectic"). In this case, HT-LSCM was applied to identify the correct present phase stabilities in the high temperature range. Based on the DSC results, the annealing temperature in the HT-LSCM was chosen to be 1300 °C. After 2 minutes of isothermal holding, further heating was performed with a heating rate of 10 °C/min. Within the range of constant heating, the material first shows a fully austenitic structure undergoing constant grain growth. At 1370 °C, the first liquid phase can be observed at the grain boundaries, attesting a hyper-peritectic behavior of alloy D-I; see Figure 8(a-III). The determined value of 1370 °C is in very good agreement with the results from the DSC measurements ($\Delta T \sim 10$ °C). Thermodynamic calculations using the assessment of Shim *et al.*[39] predict a hypo-peritectic transformation path and a significantly higher phase transformation start temperature (fcc→fcc + bcc) of 1386.59 °C, as found in the DSC measurements.

In the case of alloy D-II (0.34 pct C-0.76 pct P), first noticeable deviations from the DSC baseline are observed at 1194.2 °C. At 1457.1 °C, the sharp increase

Table V. Chemical Composition and Determined High-Temperature Phase Equilibrium Transformation Temperatures of Investigated Fe-C-0.10 Pct P and Fe-0.20 Pct C-P Ternary Alloys

Alloy	C [Mass Pct]	P [Mass Pct]	$\gamma \rightarrow \gamma + \delta$ [°C]	$\gamma + \delta \rightarrow \delta$ [°C]	$\delta \rightarrow \delta + L$ [°C]	$\gamma + \delta \rightarrow \gamma + \delta + L$ [°C]	$\gamma \rightarrow \gamma + L$ [°C]	$\gamma + L \rightarrow \gamma + \delta + L$ [°C]	$\gamma + \delta + L \rightarrow \delta + L$ [°C]	Liquidus [°C]
B-I	0.004	0.107	1359.4	1373.0	1513.9	—*	—*	—*	—*	1531.1
B-II	0.033	0.106	1380.1	1421.2	1501.8	—*	—*	—*	—*	1529.3
B-III	0.059	0.108	1401.3	1452.9	1486.8	—*	—*	—*	—*	1527.5
B-IV	0.099	0.110	1429.1	—*	—*	1471.9	—*	—*	1479.0	1524.6
B-V	0.096	0.101	1425.5	—*	—*	1472.4	—*	—*	1477.9	1525.1
B-VI	0.136	0.105	1452.4	—*	—*	1475.2	—*	—*	1482.7	1520.6
B-VII	0.203	0.106	—*	—*	—*	—*	1448.3	1480.6	1485.8	1515.9
B-VIII	0.296	0.110	—*	—*	—*	—*	1424.8	1487.6	1488.3	1507.6
B-IX	0.378	0.106	—*	—*	—*	—*	1410.6	1490.0	1490.4	1500.8
B-X	0.690	0.099	—*	—*	—*	—*	1357.7	—*	—*	1478.3
B-XI	1.000	0.099	—*	—*	—*	—*	1303.1	—*	—*	1457.8
B-XII	1.380	0.101	—*	—*	—*	—*	1234.4	—*	—*	1427.7
C-I	0.206	0.057	—*	—*	—*	—*	1460.7	1486.9	1489.8	1517.5
C-II	0.199	0.103	—*	—*	—*	—*	1445.5	1480.1	1485.9	1516.3
C-III	0.203	0.158	—*	—*	—*	—*	1428.5	1472.4	1481.5	1514.6

*Phase transformation not present according to the experimental investigations of the pseudo-binary Fe-C-P system.

in the DSC signal corresponds to the start of the peritectic phase transformation. The three-phase equilibrium (bcc + fcc + liquid) is stable only in a very small temperature interval up to 1460.3 °C. Above 1481.7 °C the alloy is in the complete liquid state. It is evident from the DSC signal and the phase diagram that alloy D-II shows a two-phase equilibrium (fcc + liquid) temperature interval of more than 250 °C, resulting in only a minor change in heat when the temperature during heating reaches the solidus line. In order to confirm the determined solidus temperature in the DSC signal of Figure 8(b-I), alloy D-II was rapidly heated up to 1175 °C in the HT-LSCM, annealed for 2 minutes and subsequently heated to an end temperature of 1325°C. Similar to alloy D-I, annealing and further heating with 10 °C/min takes place in the fully austenitic region. When reaching 1210 °C, melting of the fcc phase can be observed. The material remains in the fcc/liquid two-phase region up to the final temperature. The HT-LSCM observations again highly correlate with the DSC result of 1192.2 °C (ΔT ~ 15 °C). Calculations using the assessment of Shim *et al.*[39] give T_S = 1255.5 °C, which corresponds to a difference of more than 60 °C compared with the experimental results of the present work.

The results of samples D-III (0.68 pct C-1.275 pct P) and D-IV (1.36 pct C-2.96 pct P) are given in Figures 9(a) and (b), respectively. The sharp increase in the DSC signal of alloy D-III at 996.4 °C results from partial melting (fcc + Fe_3P→fcc + Fe_3P + liquid) of the sample. At 1002.7 °C, the reaction fcc + Fe_3P + liquid→fcc + liquid is completed according to the peak in the DSC signal. The liquidus temperature of fcc was obtained at 1421.7 °C. First melting of sample D-IV (1.36 pct C-2.96 pct P) was detected at 956.2 °C. This temperature corresponds to the eutectic phase

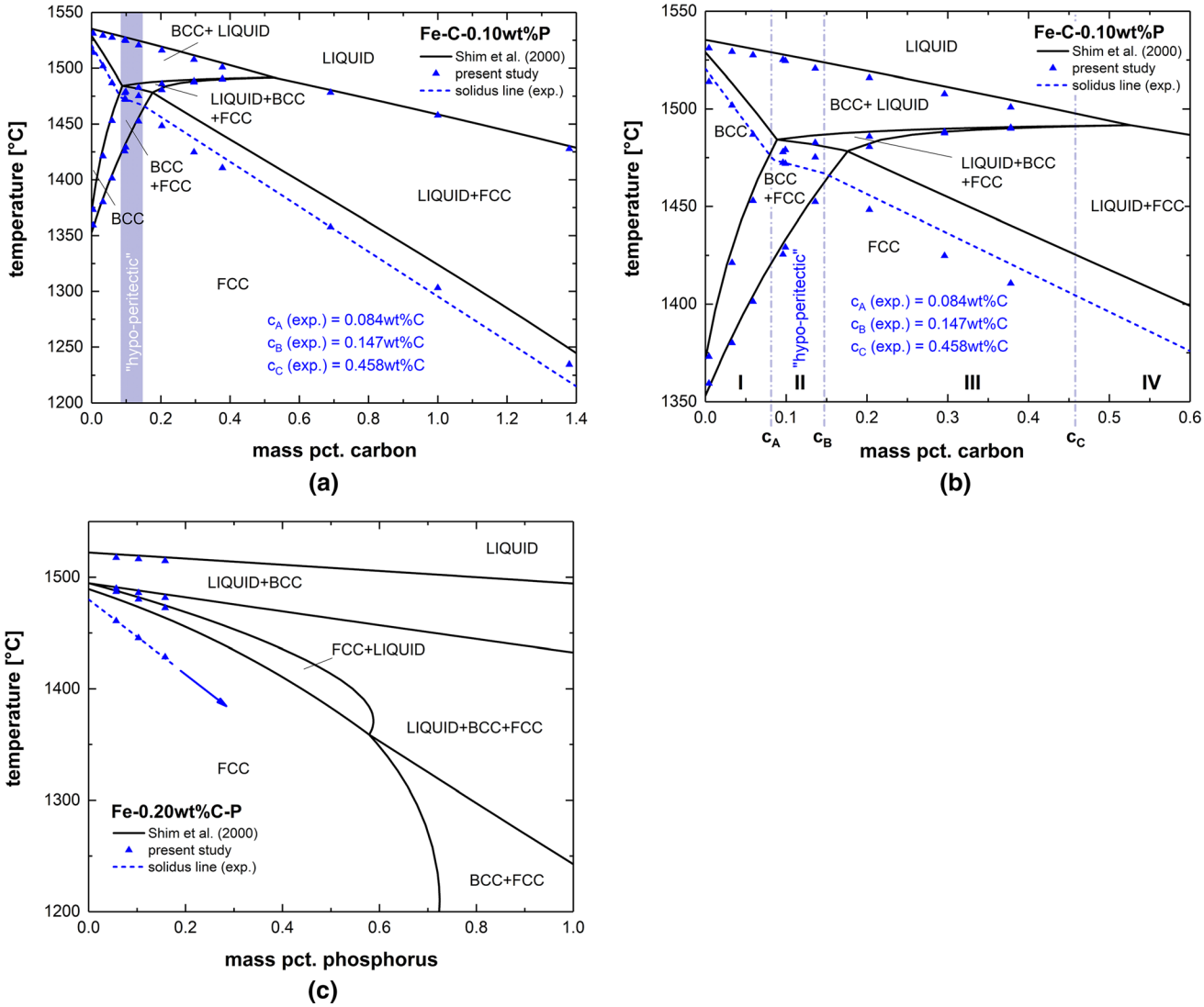

Fig. 7—Calculated vertical sections in the Fe-C-P system[39] along with present results: Fe-C-0.10 pct P (*a*), peritectic range in Fe-C-0.10 pct P (*b*) and Fe-0.20 pct C-P (*c*).

Table VI. Chemical Composition and Determined High-Temperature Phase Equilibrium Transformation Temperatures in the Fe-C-P Vertical with [pct P]/[pct C] = 2

Alloy	C [Mass Pct.]	P [Mass Pct.]	P/C Ratio [—]	$\gamma + L \rightarrow \gamma + \delta + L$ [°C]	$\gamma + \delta + L \rightarrow \delta + L$ [°C]	Solidus [°C]	Liquidus [°C]
D-I	0.170	0.430	2.53	1416.9[a]	1456.6[a]	1359.1[a] 1370.0[b]	1507.0[a]
D-II	0.340	0.760	2.24	1457.1[a]	1460.3[a]	1194.2[a] 1210.0[b]	1481.7[a]
D-III	0.680	1.275	1.88	—	—	996.4[a]	1421.7[a]
D-IV	1.360	2.960	2.18	—	—	956.2[a]	[a]

[a]Determined by the DSC method.
[b]Determined by HT-LSCM.

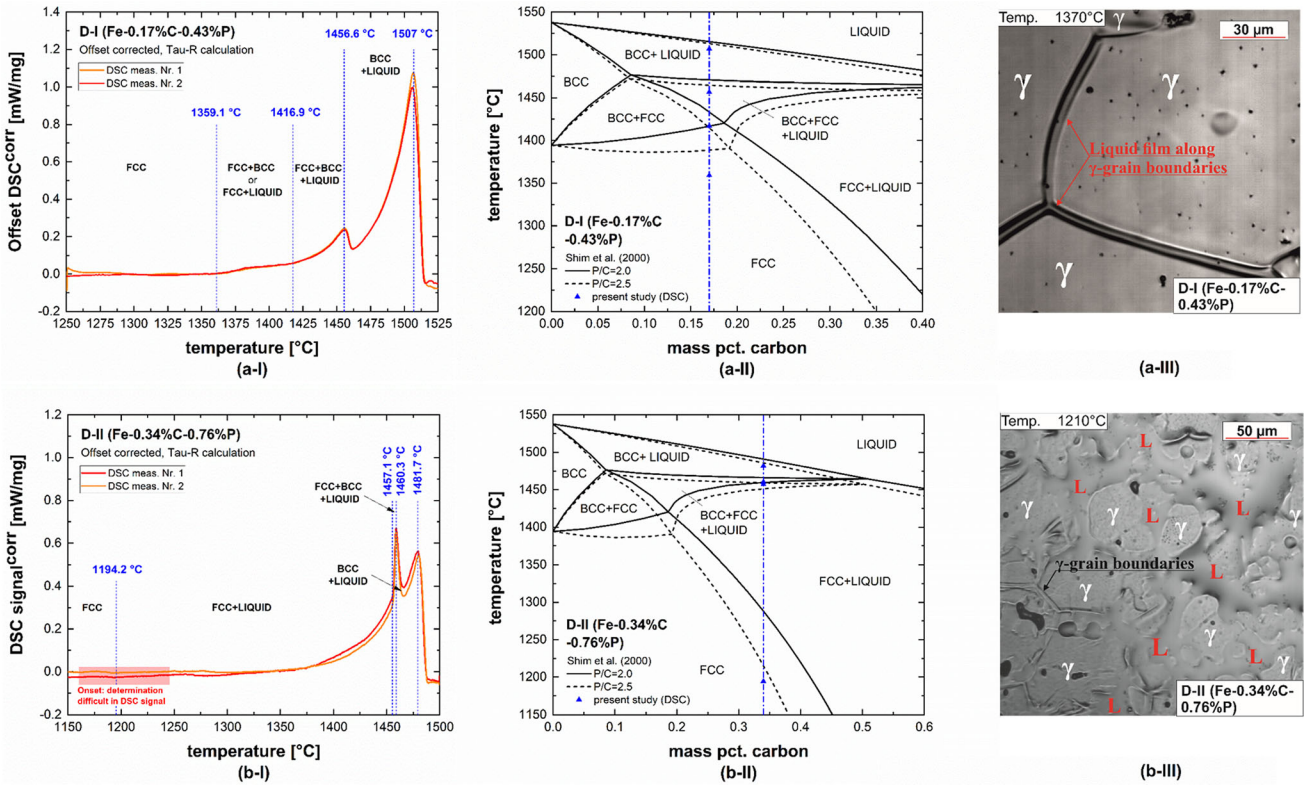

Fig. 8—Results of linking DSC and HT-LSCM for samples D-I (*a*) and D-II (*b*) showing the DSC signal (I), the calculated phase diagram along with the present experimental data (II) and the HT-LSCM observation of present phase transformations (III).

equilibrium in the ternary Fe-C-P system (fcc + Fe_3P + Fe_3C/fcc + Fe_3P + liquid) and highly correlates with the generally accepted values of 952 °C[37,39] and 955 °C.[38] Above 967.8 °C only fcc and liquid phases are stable; the liquidus temperature was found to be 1319.6 °C. In general, the phase diagrams in Figure 9 are in satisfying agreement with the DSC measurements. Particularly at temperatures lower than 1000 °C, precise prediction of phase equilibrium temperatures was achieved in the work of Shim *et al.*[39] However, higher deviations can be found at the liquidus temperature (ΔT_L~20°C). Finally, the results of samples D-I to D-IV are presented along with the calculated phase diagram in Figure 10.

V. CONCLUSION AND OUTLOOK

The purpose of the present work was to provide new phase diagram data for the improvement of thermodynamic databases and solidification models for P alloyed steel grades. Therefore, high temperature phase equilibria in the binary Fe-P system and three isoplethal sections in the ternary Fe-C-P system were characterized by means of differential scanning calorimetry (DSC). NETZSCH's Tau-R software[44,45] was critically evaluated and successfully used to optimize the efficiency of the DSC measurements by guaranteeing equilibrium conditions at the same time. The binary Fe-P subsystem was reinvestigated in the range 0.025 to 9 mass percent

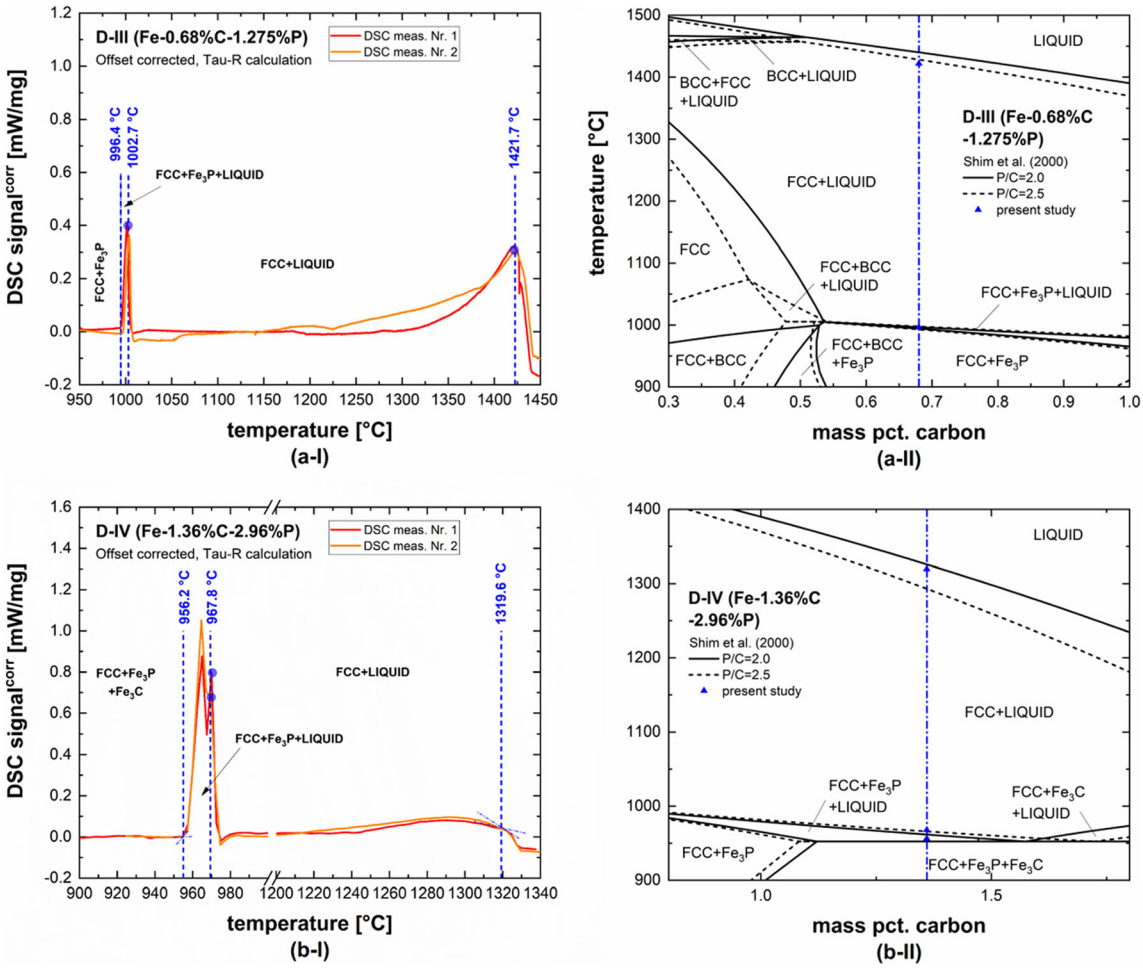

Fig. 9—Results of DSC measurements for samples D-III (*a*) and D-IV (*b*) showing the DSC signal (I) and the calculated phase diagram[39] along with the present experimental data (II).

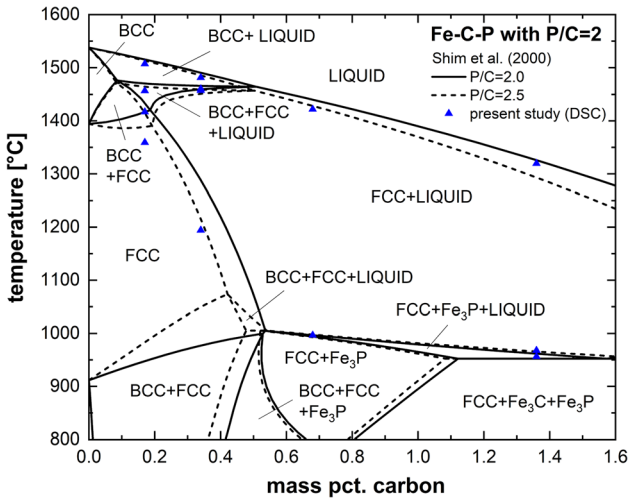

Fig. 10—Results of DSC measurements in the vertical section [pct P]/[pct C] equals 2 along with the calculated phase diagram[39] for mass pct. P/C ratios of 2 and 2.5.

P. The two isoplethal sections Fe-C-0.10 wt pct P and Fe-0.20 wt pct C-P represent the initial phosphorus composition of P alloyed steel grades, whereas a third section with constant P/C mass percent ratio of 2 corresponds to the typical interdendritic enrichments of C and P during solidification. In the latter section, selected DSC measurements were linked with high temperature laser scanning microscopy (HT-LSCM) observations to visually identify phase stabilities in the peritectic range. In the binary Fe-P system, significant differences were found between the DSC results and the most widely accepted thermodynamic assessment of Shim *et al.*[32] In the composition range [pct P] < 1, deviations up to 50 °C between the calculated and measured solidus temperatures were obtained. Although phase equilibria in the fcc/bcc gamma loop region are in high agreement with the most recent data of Fischer *et al.*[25] the experiments show inconsistencies with the calculations.[39] Similar to the binary system, experimental results in the ternary Fe-C-0.10 wt pct P and

Fe-0.20 pct C-P sections indicate higher stability of the liquid phase than that found in the optimization.[39] The experimentally determined peritectic range in the Fe-C-0.10 wt pct P section is between 0.084-0.147 mass pct. C, whereas the calculations[39] predict C composition 0.08-0.185. In the [pct P]/[pct C] equals 2 section, HT-LSCM was successfully applied to identify the present phase stabilities (fcc/bcc/liquid) within in the investigated temperature range and the observations highly correlate with results from the DSC measurements. The present experimental data can be used to refine previous thermodynamic modeling of the Fe-P and the Fe-C-P ternary system in a CALPHAD framework. The revised thermodynamic modeling of the two systems by the present authors is available elsewhere.[55] This work gives much improved thermodynamic description of the two systems, which certainly yields better prediction of thermodynamic calculation for segregation behavior in these system during casting or cooling.

ACKNOWLEDGMENTS

Open access funding provided by Montanuniversitaet Leoben. The authors gratefully acknowledge the financial support under the scope of the COMET program within the K2 Center ''Integrated Computational Material, Process and Product Engineering (ICMPPE)'' (Project No 859480). This program is supported by the Austrian Federal Ministries for Transport, Innovation and Technology (BMVIT) and for Digital and Economic Affairs (BMDW), represented by the Austrian research funding association (FFG), and the federal states of Styria, Upper Austria and Tyrol.

ELECTRONIC SUPPLEMENTARY MATERIAL

The online version of this article (https://doi.org/10.1007/s11661-020-05912-z) contains supplementary material, which is available to authorized users.

OPEN ACCESS

REFERENCES

1. M. Wintz, M. Bobadilla, and J. Jolivet: *Rev. Metall.*, 1994, vol. 91, pp. 106–14.
2. E. Schmidtmann and F. Rakoski: *Arch. Eisenhuettenwes.*, 1983, vol. 54, pp. 357–62.
3. M. Wolf and W. Kurz: *Metall. Trans. B*, 1981, vol. 12, pp. 85–93.
4. H.G. Suzuki, S. Nishimura, and Y. Nakamura: *Trans. Iron Steel Inst. Jpn.*, 1984, vol. 24, pp. 54–59.
5. X.-M. Chen, S.-H. Song, L.-Q. Weng, S.-J. Liu, and K. Wang: *Mater. Sci. Eng. A*, 2011, vol. 528, pp. 8299–04.
6. M. Yamashita, H. Miyukia, Y. Matsudaa, H. Naganoa, and T. Misawa: *Corros. Sci.*, 1994, vol. 36, pp. 283–99.
7. M. Yamashita, H. Nagano, T. Misawa, and H.E. Townsend: *ISIJ Int.*, 1998, vol. 38, pp. 285–90.
8. L. Barbé, K. Verbeken, and E. Wettinck: *ISIJ Int.*, 2006, vol. 46, pp. 1251–57.
9. P. Presoly, R. Pierer, and C. Bernhard: *Metall. Mater. Trans. A*, 2013, vol. 44A, pp. 5377–88.
10. P. Presoly, G. Xia, P. Reisinger, and C. Bernhard: *Berg- Huettenmaenn. Monatsh.*, 2014, vol. 159, pp. 430–37.
11. H. Okamoto: *Bull. Alloy Phase Diagrams*, 1990, vol. 11, pp. 404–12.
12. W. Franke, K. Meisel, and R. Juza: *Z. Anorg. Chem.*, 1934, vol. 218, pp. 346–59.
13. K. Meisel: *Z. Anorg. Chem.*, 1934, vol. 218, pp. 360–64.
14. M. Heimbrecht and W. Biltz: *Z. Anorg. Chem.*, 1939, vol. 242, pp. 233–36.
15. W. Jeitschko and D.J. Braun: *Acta Crystallogr. B*, 1978, vol. 34, pp. 3196–3201.
16. B. Saklatwalla: *J. Iron Steel Inst.*, 1908, vol. 77, pp. 92–103.
17. N. Konstantinow: *Z. Anorg. Chem.*, 1910, vol. 66, pp. 209–27.
18. J.L. Houghton: *J. Iron Steel Inst.*, 1927, vol. 115, pp. 417–33.
19. R. Vogel: *Arch. Eisenhuettenw.*, 1929, vol. 3, pp. 369–81.
20. E. Wachtel, G. Urbain, and E. Übelacker: *C.R.*, 1963, vol. 257, pp. 2470–72.
21. E. Schürmann: *Arch. Eisenhuettenw.*, 1980, vol. 51, pp. 325–27.
22. Z.I. Morita and T. Tanaka: *Trans. Iron Steel Inst. Jpn.*, 1986, vol. 26, pp. 114–20.
23. P. Roquet and G. Jegaden: *Rev. Metall.*, 1951, vol. 48, pp. 712–21.
24. K. Lorenz and H. Fabritius: *Arch. Eisenhuettenw.*, 1962, vol. 33, pp. 269–75.
25. W.A. Fischer, K. Lorenz, H. Fabritius, A. Hoffmann, and G. Kalwa: *Arch. Eisenhuettenw.*, 1966, vol. 37, pp. 79–86.
26. H. Kaneko, T. Nishizawa, K. Tamaki, and A. Tanifuji: *J. Japan. Inst. Metals*, 1965, vol. 29, pp. 166–70.
27. A.S. Doan and J.I. Goldstein: *Metall. Trans.*, 1970, vol. 1, pp. 1759–67.
28. H.P. Hofmann, K. Löhberg, and W. Reif: *Arch. Eisenhuettenw.*, 1970, vol. 41, pp. 975–82.
29. M. Ko and T. Nishizawa: *J. Jpn. Inst. Met.*, 1979, vol. 43, pp. 118–26.
30. P. Spencer and O. Kubaschewski: *Arch. Eisenhuettenwes.*, 1978, vol. 49, pp. 225–28.

31. P. Gustafson, Report IM-2549, Swedish Institute for Metals Research, Stockholm, Sweden, 1990.
32. J.H. Shim, C.S. Oh, and D.N. Lee: *J. Korean Inst. Met. Mater.*, 1996, vol. 34, pp. 1385–93.
33. H. Ohtani, N. Hanaya, M. Hasebe, S.-I. Teraoka, and M. Abe: *Calphad*, 2006, vol. 30, pp. 147–58.
34. T. Tokunaga, N. Hanaya, H. Ohtani, and M. Hasebe: *Mater. Sci. Forum*, 2007, vols. 561–565, pp. 1899–1902.
35. Z.-M. Cao, K.-P. Wang, Z.-Y. Qiao, and G.-W. Du: *Acta Phys. Chim. Sin.*, 2012, vol. 28, pp. 37–43.
36. J. Miettinen and G. Vassilev: *Phase Equilib. Diffus.*, 2014, vol. 35, pp. 458–68.
37. P. Perrot, Landolt-Börnstein—Group IV Physical Chemistry Volume 11D2: "Iron Systems, Part 2", Springer Materials, Springer, Berlin Heidelberg, 2008. https://doi.org/10.1007/978-3-540-74196-1_11.
38. E. Schürmann, U. Hensgen, and J. Schweinichen: *Giessereiforschung*, 1984, vol. 36, pp. 121–29.
39. J.-H. Shim, C.-S. Oh, and D.N. Lee: *Z. Metallkd.*, 2000, vol. 91, pp. 114–20.
40. P. Gustafson: *Scand. J. Metall.*, 1985, vol. 14, pp. 259–67.
41. G.W. Höhne, H.W. Hemminger, and H.J. Flemmingheim: *Differential Scanning Calorimetry: An Introduction to Practitioners*, 1st ed., Springer, Berlin, 1996.
42. W. J. Boettinger, U. R. Kattner, K.-W. Moon and J. H. Perepezko, DTA and Heat-flux DSC measurements of Alloy Melting and Freezing. NIST Recommended Practice Guide, Special Publication 960-15, 2006.
43. L.A. Chapman: *J. Mater. Sci.*, 2004, vol. 39, pp. 7229–36.
44. Software: NETZSCH Tau-R Calibration 8.0.1 from Netzsch Gerätebau GmbH, Selb, Germany, 2019.
45. E. Moukhina and E. Kaisersberger: *Thermochim. Acta*, 2009, vol. 492, pp. 101–109.
46. W.J. Boettinger and U.R. Kattner: *Metall. Mater. Trans. A*, 2002, vol. 33A, pp. 1779–94.
47. M. Reid, D. Phelan, and R. Dippenaar: *ISIJ Int.*, 2004, vol. 44, pp. 565–72.
48. C. Bernhard, S. Schider, A. Sormann, G. Xia, and S. Ilie: *Berg-Huettenmaenn. Monatsh*, 2011, vol. 156, pp. 161–67.
49. S. Griesser and R. Dippenaar: *ISIJ Int.*, 2014, vol. 54, pp. 533–35.
50. N. Fuchs, P. Krajewski, and C. Bernhard: *Berg-Huettenmaenn. Monatsh.*, 2015, vol. 160, pp. 214–20.
51. C.W. Bale, E. Bélisle, P. Chartrand, S.A. Decterov, G. Eriksson, A.E. Gheribi, K. Hack, I.-H. Jung, Y.-B. Kang, J. Melançon, A.D. Pelton, S. Petersen, C. Robelin, J. Sangster, P. Spencer, and M.-A. van Ende: *Calphad*, 2016, vol. 54, pp. 35–53.
52. A. Grill and J.K. Brimacombe: *Ironmak. Steelmak.*, 1976, vol. 3, pp. 76–79.
53. Y. Maehara, K. Yasumoto, H. Tomono, T. Nagamichi, and Y. Ohmori: *Mater. Sci. Technol.*, 1990, vol. 6, pp. 793–806.
54. G. Xia, C. Bernhard, S. Ilie and C. Fürst, Proceedings of the 6th European Conference on Continuous Casting 2008, Riccione, Italy, 2008.
55. M. Bernhard, Y.-B. Kang, P. Presoly, A.E. Gheribi, and C. Bernhard: *Calphad*, 2020, vol. 70, art. no. 101795.